HHS Public Access

Author manuscript

Cell Rep. Author manuscript; available in PMC 2021 May 21.

Published in final edited form as:

Cell Rep. 2021 May 04; 35(5): 109074. doi:10.1016/j.celrep.2021.109074.

Dysregulation of the mesoprefrontal dopamine circuit mediates an early-life stress-induced synaptic imbalance in the prefrontal cortex

Won Chan Oh[1,2,*], **Gabriela Rodríguez**[1], **Douglas Asede**[1], **Kanghoon Jung**[1,3], **In-Wook Hwang**[2], **Roberto Ogelman**[2], **McLean M. Bolton**[1], **Hyung-Bae Kwon**[1,3,4,5,*]

[1]Max Planck Florida Institute for Neuroscience, Jupiter, FL 33458, USA

[2]Department of Pharmacology, University of Colorado School of Medicine, Anschutz Medical Campus, Aurora, CO 80045, USA

[3]Department of Neuroscience, Johns Hopkins University School of Medicine, Baltimore, MD 21205, USA

[4]Max Planck Institute of Neurobiology, Martinsried 82152, Germany

[5]Lead contact

SUMMARY

Stress adversely affects an array of cognitive functions. Although stress-related disorders are often addressed in adulthood, far less is known about how early-life stress (ELS) affects the developing brain in early postnatal periods. Here we show that ELS, induced by maternal separation, leads to synaptic alteration of layer 2/3 pyramidal neurons in the prefrontal cortex (PFC) of mice. We find that layer 2/3 neurons show increased excitatory synapse numbers following ELS and that this is accompanied by hyperexcitability of PFC-projecting dopamine (DA) neurons in the ventral tegmental area. Notably, excitatory synaptic change requires local signaling through DA D2 receptors. *In vivo* pharmacological treatment with a D2 receptor agonist in the PFC of control mice mimics the effects of ELS on synaptic alterations. Our findings reveal a neuromodulatory mechanism underlying ELS-induced PFC dysfunction, and this mechanism may facilitate a more comprehensive understanding of how ELS leads to mental disorders.

Graphical Abstract

[*]Correspondence: wonchan.oh@cuanschutz.edu (W.C.O.), hkwon29@jhmi.edu (H.-B.K.).

AUTHOR CONTRIBUTIONS

W.C.O. and H.-B.K. conceived and designed the study. W.C.O. performed and analyzed all experiments except behavioral studies and immunohistochemistry. G.R. and W.C.O. performed and analyzed dopamine receptor pharmacological studies. D.A., M.M.B., and K.J. performed and analyzed behavioral assays. K.J. performed and analyzed immunohistochemistry. I.-W.H. and R.O. helped with pharmacological studies and data analysis. W.C.O. prepared the figures. W.C.O. and H.-B.K. wrote the manuscript. All authors revised the manuscript.

SUPPLEMENTAL INFORMATION

Supplemental information can be found online at https://doi.org/10.1016/j.celrep.2021.109074.

DECLARATION OF INTERESTS

The authors declare no competing interests.

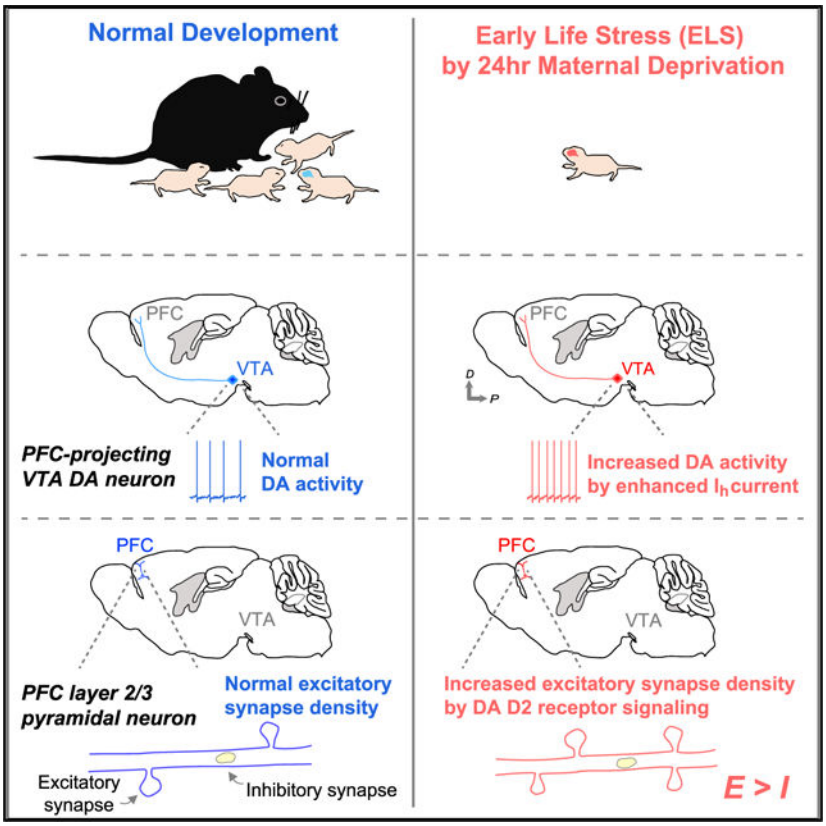

In brief

Oh et al. demonstrate developmental perturbation of the excitatory/inhibitory balance in the prefrontal cortex (PFC) caused by early-life stress (ELS). The alteration is mediated by hyperexcitability of PFC-projecting dopamine neurons and D2 receptor signaling in the PFC. These findings highlight cellular mechanisms by which ELS leads to brain dysfunction.

INTRODUCTION

Children who have experienced early-life stress (ELS), such as physical and emotional neglect or abuse during a critical period, are at higher risk for mental health disorders later in life, such as autism spectrum disorder (ASD) and major depressive disorder (MDD) (Kessler et al., 1997; Rentesi et al., 2013; Wang et al., 2014). Understanding the neurobiological mechanisms that transduce ELS into altered neural activity during development that results in behavioral deficits in adulthood is essential for development of psychological and pharmacological treatments to improve outcomes for these individuals. However, most of the studies of stress have focused on stress-induced behavioral dysfunction or chronic stress effects on adult psychopathology (Arnsten, 2009, 2015; Tost et al., 2015); little is known about its effect on basic cortical and synaptic functions in the developing brain.

Plasticity of neuronal structure, such as growth and retraction of excitatory synapses, is thought to contribute to the experience-dependent changes in neural circuitry that mediate learning and memory (Bosch and Hayashi, 2012; Holtmaat and Svoboda, 2009).

Manipulations that drive experience-dependent circuit plasticity *in vivo* have been associated with formation and elimination of dendritic spines during development and learning (Chen et al., 2015; Holtmaat and Svoboda, 2009; Holtmaat et al., 2006; Peters et al., 2014; Tschida and Mooney, 2012; Xu et al., 2009). Prolonged exposure to aversive experiences also leads to structural changes (Chen et al., 2018; Shu and Xu, 2017). Stressed animals exhibit dendritic retraction and spine loss in the hippocampus, sensory cortex, and prefrontal cortex (PFC) (Chen et al., 2018; Kim and Diamond, 2002; Radley et al., 2008). Specifically, the PFC, which plays a critical role in higher-order cognition, is highly sensitive to stress compared with other brain areas (Arnsten, 2009, 2015). Past studies of structural and functional changes in the PFC have shown that dendrites and spines in layer 2/3 and layer 5 pyramidal neurons are eliminated after only 7–10 days of stress (Brown et al., 2005; Shu and Xu, 2017). Even a single transient exposure to an aversive cue causes dendritic retraction in the PFC (Izquierdo et al., 2006). Notably, the PFC receives major dopaminergic (DAergic) synaptic inputs from the ventral tegmental area (VTA), and VTA dopamine (DA) neurons increase their firing to aversive stimuli, leading to higher levels of DA release in the PFC during stress (Deutch and Roth, 1990; Lammel et al., 2014). These data suggest that dysregulation of DAergic neurons in the VTA that project to the PFC may underlie the pathophysiology in stress-induced PFC dysfunction. Although these studies provided valuable insights into the aversive effect of stress on the PFC and how they relate to mental disorders, all studies were performed on adult animals. Therefore, information is lacking about how synapse development in the PFC is altered by ELS in early postnatal stages, a period when experience-dependent neural plasticity is at its peak.

We use two-photon microscopy, electrophysiology, and the early maternal separation stress paradigm to address the neural mechanisms by which ELS drives synaptic alteration in the developing PFC.

RESULTS

ELS increases excitatory synapse density of layer 2/3 pyramidal neurons in the PFC

To determine how ELS affects the developing PFC, we adopted the early maternal separation stress paradigm. This manipulation disrupts early social bonding by exposing pups to a single 24-h episode of mother/littermate deprivation on postnatal day 8 (P8) (Authement et al., 2015). Using a three-chamber social preference test in young adult mice (8–9 weeks), which quantifies a mouse's preference for investigating a novel mouse versus an object (Shin et al., 2018; Silverman et al., 2010), we verified this stress paradigm and found that ELS mice exhibit significantly reduced social preference compared with control mice (Figures S1A–S1C) with no accompanying change in anxiety behaviors (Figures S1D–S1F). These results suggest a detrimental effect of adverse early-life experiences on PFC function, which may precede social behavioral deficits in adulthood (Yizhar et al., 2011).

In adult mice, stress-induced dendritic retraction and spine loss have been observed in the PFC (Cook and Wellman, 2004; Radley et al., 2004; Shu and Xu, 2017). We therefore examined whether ELS leads to structural alterations of excitatory synapses on layer 2/3 pyramidal neurons in the PFC shortly after maternal separation (Figure 1A). In contrast to previous studies in adult mice, we found that ELS pups showed significantly increased

dendritic spine density on layer 2/3 pyramidal neurons in the dorsal PFC (Figures 1A–1C). Neither spine size nor morphology were affected by ELS (Figure 1D). Enhanced spine density in the PFC was not due to overall deterioration of brain structure caused by ELS because spine density in the somatosensory cortex (SSC) of ELS mice was comparable with that of controls (Figures 1B and 1C). To assess whether the change in spine density reflected functional alterations, acute slices from P9–P10 ELS and control pups were used for whole-cell patch-clamp experiments. Consistent with structural changes, ELS exposure significantly increased the frequency but not amplitude of miniature excitatory postsynaptic currents (mEPSCs) (Figures 1E and 1F), whereas neither the miniature inhibitory postsynaptic current (mIPSC) frequency nor amplitude changed in ELS mice (Figure 1G). These results indicate that ELS selectively increases excitatory synapse density on layer 2/3 pyramidal neurons in the PFC during early postnatal development, suggesting an increase in the prefrontal synaptic excitation to inhibition ratio after ELS.

ELS increases the activity of PFC-projecting mesocortical DA neurons in the VTA

What neural mechanisms transduce ELS into altered synaptic activity in the PFC? Multiple lines of evidence suggest that the mesoprefrontal DAergic circuit responds to aversive stimuli (Arnsten, 2009; Lammel et al., 2011). Cortical DAergic innervation is largely confined to areas of the frontal cortex, whereas the sensory cortices receive very sparse DA afferents (Berger et al., 1991; Jacob and Nienborg, 2018). Because ELS-induced synaptic change was evident in the PFC but absent in the SSC (Figures 1B and 1C), we wanted to find out whether and how PFC-projecting mesocortical VTA DA neurons are affected by ELS. Using Cre-dependent viral expression strategies with transgenic mice expressing Cre recombinase under the control of the DA transporter (DAT) promoter, we verified that mesocortical DAergic neurons in the VTA form widely spread and highly dense axonal arborizations in the developing PFC *in vivo* (Figures S2A–S2C). In a separate set of experiments, we injected retrogradely transported, fluorescently labeled latex microspheres (RetroBeads, Lumafluor) into the dorsal PFC of pups at P1 to selectively target and examine PFC-projecting VTA DA neurons (Figure S2D). In this scheme, RetroBead-positive cells in the VTA indicate PFC-projecting putative DA neurons. We recorded from RetroBead-positive neurons (Figure S2E) and observed that mesoprefrontal DA neurons from ELS mice exhibited hyperexcitability (Figures 2A–2C), consistent with previous reports of adult mice (Lammel et al., 2014). The resting membrane potential and spiking threshold were unaffected (Figures 2D and 2E). However, we found that PFC-projecting VTA DA neurons exhibited upregulated hyperpolarization-activated cation channel-mediated current (I_h), an excitatory driving force in VTA DA neurons (Figures 2F and 2G). These findings demonstrate that ELS increases the excitatory I_h current in mesoprefrontal VTA DA neurons, resulting in hyperexcitability of these cells.

Alterations in prefrontal excitatory synapses and the mesoprefrontal DA system following ELS are long lasting

Previous reports indicated that chronic stress in adult mice causes long-lasting changes in VTA DA neuronal activity (Polter and Kauer, 2014) and structural alterations in the dendrites of prefrontal cortical pyramidal neurons (Cook and Wellman, 2004; Radley et al., 2008). It remains unclear, however, whether exposure to a single period of early adversity

leads to long-term synaptic changes in the PFC and the activity of the PFC-projecting DA neuromodulatory circuit. We therefore examined the long-lasting effects of ELS on excitatory synapses in the PFC and the intrinsic excitability of VTA DA neurons. We found that a single ELS at P8 leads to a long-lasting increase in excitatory but not inhibitory synapse density on prefrontal layer 2/3 pyramidal neurons (Figures 3A–3D) and a persistent increase in intrinsic excitability of VTA DA neurons at P17–P21 (Figures 3E–3G). In addition, we observed that hyperexcitability of mesoprefrontal DA neurons was caused by enhanced I_h current (Figures 3H and 3I) without changes in the resting membrane potential or the threshold potential for spikes (Figures 3J and 3K). Sex differences in response to ELS were not observed (Figures 3L–3N). These results indicate that acute ELS drives long-lasting enhancement of VTA DA neuron excitability, potentially increasing DA release in the PFC, where significantly increased excitatory synapses were observed.

DA D2 receptor signaling mediates ELS-induced enhancement of excitatory synapse density

In vivo microdialysis studies examining extracellular DA following stressful stimuli have found a robust DA increase in VTA projection targets, including the PFC (Holly and Miczek, 2016; Lammel et al., 2014). We hypothesized that DA signaling in the PFC may be responsible for the ELS-induced synaptic alteration. To examine this hypothesis, we eliminated DAergic terminals in the PFC by local injection of the neurotoxin 6-hydroxydopamine (6-OHDA; 9 μg; Figure S3) into P1 pups. We found that spine density was decreased significantly following 6-OHDA injection into the PFC but not SSC of control mice (Figures 4A–4D). A significant reduction in mEPSC frequency was also observed in 6-OHDA-injected control mice (Figures 4E and 4F). Intriguingly, no further enhancement of spine density or mEPSC frequency was observed in ELS mice injected with 6-OHDA (Figures 4A–4F). This lack of ELS effects on excitatory synapses was not due to the effect of 6-OHDA lesions on mouse health because spine density in the SSC of 6-OHDA-injected mice was comparable with that of vehicle-injected controls (Figure 4D), and 6-OHDA injected pups showed normal feeding and locomotor behaviors (Figure S4). These data suggest that endogenous DA is critical for PFC development in early postnatal stages. Additionally, it indicates that ELS increases the density of excitatory synapses primarily through local mechanisms involving mesocortical DAergic projections in the PFC. This led us to further examine how distinct DA receptor signaling selectively contributes to ELS-induced abnormal synapse development in the PFC. We microinjected the D1 receptor antagonist SCH23390 (1 μg) or D2 receptor antagonist haloperidol (5 μg) or eticlopride (5 μg) directly into the PFC during ELS and measured mEPSCs from vehicle- and drug-injected ELS mice at P9–P10 (Figure 4G). We found that ELS mice treated with SCH23390 exhibited an increased mEPSC frequency similar to that in vehicle-treated ELS mice (Figure 4H). However, blockade of D2 receptors with haloperidol or eticlopride completely abolished ELS-mediated enhancement of mEPSC frequency without affecting mEPSC amplitudes (Figures 4I and 4J). To further confirm the involvement of DA D2 receptors in excitatory synaptic change in ELS mice, we examined whether D2 receptor activation could increase excitatory synapses in control mice. We locally injected a D2 receptor agonist, quinpirole (2.5 μg), into the PFC at P8 and found that quinpirole-treated control mice mimicked the changes in excitatory synapse density observed in ELS mice (Figures 4K–

4M). These data strongly suggest that upregulation of DA D2 receptor signaling via enhanced mesoprefrontal DA neuron activity contributes to the increased excitatory synapses on layer 2/3 pyramidal neurons in the PFC after ELS.

DISCUSSION

The early postnatal period is a critical stage during which the brain undergoes robust circuit remodeling (Katz and Shatz, 1996; Kolb et al., 2012). Formation, elimination, and plasticity of spine synapses are key components of neural circuit plasticity (Kwon and Sabatini, 2011; Oh et al., 2013, 2016; Spruston, 2008). Thus, any environmental factor that can affect the developing brain can have a long-lasting effect on synaptic structure and function (Lupien et al., 2009). Previous studies have found a link between early adversity and a later propensity to develop mental health disorders (Bick and Nelson, 2016; Rentesi et al., 2013; Shin et al., 2018; Yizhar et al., 2011).

Studies using maternal deprivation (MD) paradigms have shown several neural mechanisms for adverse outcomes (Authement et al., 2015; Lupien et al., 2009; Shin et al., 2018). A single instance of MD is thought to induce long-term depression (LTD) at inhibitory synapses onto VTA DA neurons through epigenetic mechanisms (Authement et al., 2015). In adult mice, aversive events have been shown to excite DA neurons and increase DA release in target structures, including the PFC (Lammel et al., 2014). The PFC has a prolonged developmental period, starting its maturation perinatally and extending high levels of plasticity into adolescence (Kolb et al., 2012), making it more susceptible to environmental insults. These observations raise the possibility that DAergic circuits might be involved in the various aspects of ELS-induced PFC dysfunction. Here we employed a single episode of the MD paradigm and found that dysregulation of mesoprefrontal VTA DA neurons is a neural mechanism by which ELS alters excitatory synapses in the PFC.

How does ELS lead to hyperactivity in mesoprefrontal VTA DA neurons? ELS could directly modify excitatory synapses on DA neurons, resulting in an increase in synaptic strength and activity (Lammel et al., 2011). Another possibility could be that ELS induces GABAergic synaptic alteration, shifting the balance of glutamatergic/GABAergic synaptic inputs toward a reduction of inhibition and, thus, increases DA neuronal excitability (Authement et al., 2015). Stress-modulating signaling molecules, such as corticotropin-releasing factor (CRF), might also promote firing in DA neurons (Wanat et al., 2008). We found significant upregulation of I_h current in PFC-projecting VTA DA neurons of ELS mice, and increased I_h and hyperactivity in VTA DA neurons are thought to underlie the susceptible phenotype of social defeat stress depression (Friedman et al., 2014).

Increased excitatory synapse density on prefrontal pyramidal neurons following ELS was not dependent on DA D1 receptors but was affected by D2 receptor signaling. Considerable evidence supports that DA acting on D1-like receptors increases NMDA receptor (NMDAR) currents, membrane depolarization, cytosolic Ca^{2+} levels, and surface AMPA receptors through protein kinase A (PKA) and protein kinase C (PKC) (Money and Stanwood, 2013; Tritsch and Sabatini, 2012). On the other hand, D2 receptors reduce PKA activity and limit Ca^{2+}-dependent signaling mechanisms (Money and Stanwood, 2013; Tritsch and Sabatini,

2012). Multiple studies demonstrate that synaptogenesis is dependent on NMDA receptor and PKA signaling (Hamilton et al., 2012; Kwon and Sabatini, 2011), suggesting a potential role of D1 receptors in synaptic alteration of ELS mice. Surprisingly, however, we found that D2 receptors play a selective role in mediating synaptic changes in the PFC following ELS.

D2 receptors are known to be localized in the presynaptic terminal of DA neurons and inhibit DA release via an autoregulation loop (Burke and Miczek, 2014; Weber et al., 2018). This presynaptic inhibition may intuitively predict inhibition of excitatory synapse formation. However, the D2 family of DA receptors is also present in the postsynapses of PFC pyramidal neurons (Clarkson et al., 2017). Recent studies suggest a new model where D2 receptors act via Gs- but not $G_{i/o}$-mediated signaling to stimulate PKA and elicit excitability in the PFC (Robinson and Sohal, 2017). In addition, endocytosis following D2 receptor activation has been shown to increase spine formation and neuronal activity in the striatum (Shioda et al., 2017). Therefore, combination of pre- and post-synaptic D2 receptor activation, potential involvement of DA/glutamate co-release, and the change in DA neuron firing should be considered together when interpreting the current results.

Our study suggests that ELS can alter the synaptic excitation-inhibition ratio in prefrontal pyramidal neurons primarily through DA D2 receptor signaling. Our findings reveal a functional role of the mesoprefrontal DAergic circuit in mediating the detrimental effects of adverse early life experiences on PFC dysfunction. This is a significant advance in our understanding of the neural mechanisms by which ELS leads to long-lasting modification of a specific neural circuit and causes cortical and synaptic alterations in the developing PFC. Our results may provide a mechanistic basis for a set of novel therapeutic strategies to treat mental health disorders induced by early adversity.

STAR★METHODS

RESOURCE AVAILABILITY

Lead contact—Further information and requests for resources and reagents should be directed to the Lead Contact, Hyung-Bae Kwon (hkwon29@jhmi.edu)

Materials availability—This study did not generate new unique reagents.

Data and code availability—This study did not generate datasets/code.

EXPERIMENTAL MODEL AND SUBJECT DETAILS

Early Life Stress Procedure—All experiments were performed in accordance with protocols approved by the Institutional Animal Care and Use Committees of the Max Planck Florida Institute for Neuroscience and the University of Colorado on Anschutz Medical Campus and National Institutes of Health guidelines. A minimum of 3 mice per each group were used for each experimental comparison. The 24-hour maternal separation paradigm was adopted from previously described methods with minor modifications (Authement et al., 2015). Briefly, pups were taken from the dam and littermates at P8 and individually isolated for 24 hours in a chamber with clean bedding on heating pads maintained at 37°C. The corner of bedding was moistened with water. ELS pups were not disturbed during separation

and returned to the home cage at P9 right after 24-hour ELS procedure. Litter-, age-, and gender-matched control pups remained undisturbed in the maternal nest. Both female and male pups were used.

Preparation of acute brain slices—Acute coronal cortical slices including the PFC or midbrain slices containing the VTA were prepared from C57BL/6 wild-type or DAT-IRES-Cre (DAT-Cre) heterozygous mice (Jackson Laboratory stock 006660). Mice were anesthetized with isoflurane and killed by decapitation. The brain was removed from the skull and rapidly placed in ice-cold cutting solution containing (in mM): 215 sucrose, 20 glucose, 26 $NaHCO_3$, 4 $MgCl_2$, 4 $MgSO_4$, 1.6 NaH_2PO_4, 1 $CaCl_2$ and 2.5 KCl. Cortical slices (300 μm thick) were prepared using a VT1000S vibrating microtome (Leica). Slices were incubated at 32°C for 30 minutes in a holding chamber containing 50% cutting solution and 50% artificial cerebrospinal fluid (ACSF) containing (in mM): 124 NaCl, 26 $NaHCO_3$, 10 glucose, 2.5 KCl, 1 NaH_2PO_4, 2.5 $CaCl_2$, and 1.3 $MgSO_4$. After 30 minutes, this solution was slowly replaced with ACSF at room temperature. Slices were allowed to recover for 1 hour in ACSF before recording or imaging. For electrophysiology and two-photon imaging experiments, slices were transferred to a submersion-type, temperature-controlled recording chamber (TC-344B, Warner Instruments) and perfused with ACSF. All solutions were equilibrated for at least 30 min with 95%O_2/5%CO_2.

METHOD DETAILS

Two-photon imaging—Slice two-photon imaging was performed on transfected layer 2/3 pyramidal neurons within 40 μm of the slice surface at 30°C in recirculating ACSF. For *in vivo* two-photon imaging, 2–3 mm craniotomy was made and a customized anodized cone-shape *in vivo* chamber was attached to the skull around the craniotomy site and fixed by dental cement. *In vivo* chamber was firmly affixed to the head plate connected to the head post at the stage. Mice were anesthetized with the cocktail of ketamine and xylazine (0.1 mg/0.01 mg/g) during surgery and experiment. For each neuron, image stacks (512 × 512 pixels; 0.035 μm / pixel) with 1-μm z-steps were collected from a segment of secondary or tertiary apical and/or basal dendrites (average of five dendrites per cell) using a two-photon microscope (Bruker, Inc) with a pulsed Ti::sapphire laser (MaiTai HP DeepSee, Spectra Physics) tuned to 920 nm (3–5 mW at the sample).

Intracranial injections—Viruses, fluorescent retrobeads, and drugs were injected into the dorsolateral prefrontal cortex (DL-PFC covering FrA region) in a stereotactic setup (Kopf instruments, Tujunga, CA, USA). Neonate mice (P0–1) were cryoanesthetized. Following cessation of movement, a solution of recombinant adeno-associated virus (AAV) diluted in sterile phosphate-buffered saline (PBS) was injected bilaterally into layer 2/3 prefrontal cortex using a pulled glass needle (30–40 μm). The needle was held perpendicular to the skull surface during insertion to a depth of approximately 200–300 μm. Once the needle was in place, viral solution was manually injected. 200–500 nL injections were used for tdTomato expression (pAAV-CAG-tdTomato, a gift from Edward Boyden, Addgene plasmid # 59462). Seven to 21 days after viral injection, 2–3 mm craniotomy was carried out for *in vivo* imaging and acute cortical slices were made for slice imaging or electrophysiology. For retrobead labeling (LumaFluor Inc.), neonates were treated as described above except that

200 nL of retrobeads were injected. Eight to 21 days after retrobead injection, coronal midbrain slices (300 μm thick) containing the ventral tegmental area (VTA) were prepared and retrobead-labeled putative DA neurons in the paranigral nucleus (PN) of the medial posterior VTA were visually identified for electrophysiology experiments. For selective labeling of VTA DA neurons, 500 nL injections of viral solution were used for tdTomato expression (AAV1-CAG-Flex-tdTomato-WPRE-bGH) using DAT-IRES-Cre (DAT-Cre) heterozygous pups (Jackson Laboratory stock 006660). *In vivo* pharmacological manipulation was performed on mouse pups. P1 pups were cryoanesthetized and 6-hydroxydopamine (9 μg per hemisphere) was locally injected in DL-PFC. P8 pups were anesthetized and head-fixed on a stereotaxic device with constant administration of 3% isoflurane/oxygen mix and DL-PFC was targeted for intracerebral microinjections of SCH23390 (1 μg per hemisphere, twice per day), haloperidol (5 μg per hemisphere, once per day), eticlopride (5 μg per hemisphere, once per day), or quinpirole (2.5 μg per hemisphere, twice per day). One to 2 days after intracranial drug injection, acute coronal cortical slices including the DL-PFC were prepared and pyramidal neurons in layer 2/3 of the PFC were targeted for electrophysiology and two-photon imaging. Control subjects received the same amount of vehicle solution. Once injected, pups were allowed to recover on a heating pad until movement was restored.

Electrophysiology—Whole-cell recordings (electrode resistances 4–8 MΩ; series resistances 20–40 MΩ) were performed on visually identified layer 2/3 pyramidal neurons or VTA DA neurons within 40 μm of the slice surface using a MultiClamp 700B amplifier (Molecular Devices). Spontaneous miniature excitatory postsynaptic current (mEPSC) was measured at 30°C in voltage-clamp configuration (Vhold = −65 mV) using cesium-based internal solution in ACSF containing (in mM): 2 Ca^{2+}, 1 Mg^{2+}, 0.001 TTX, 0.01 CPP, and 0.01 Bicuculline. For spontaneous miniature inhibitory postsynaptic current (mIPSC) recording, layer 2/3 neurons were patched at 30°C in voltage-clamp configuration (Vhold = +10 mV) using cesium-based internal solution in ACSF containing (in mM): 2 Ca^{2+}, 1 Mg^{2+}, 0.001 TTX, 0.01 CPP, and 0.01 NBQX. To examine spiking properties, whole-cell properties were recorded in current-clamp mode using potassium-based internal solution (in mM: 136 K-gluconate, 10 HEPES, 17.5 KCl, 9 NaCl, 1 $MgCl_2$, 4 Na_2-ATP, 0.4 Na-GTP, and ~300 mOsm, ~pH 7.26) at 30°C in ACSF containing 2 mM Ca^{2+} and 1 mM Mg^{2+}. Action potential firing rates were measured by injecting depolarizing current steps (15–200 pA, 1 s). Hyperpolarization-activated cation (I_h) currents were measured at 30°C in voltage-clamp configuration with a 1 s pulse of voltage step from −130 mV to −65 mV from a holding potential at −65 mV using potassium-based internal solution in ACSF containing 2 mM Ca^{2+} and 1 mM Mg^{2+}. Signals were filtered at 2 kHz and digitized at 10 kHz and responses were analyzed using Clampfit 10.3 (Molecular Devices) and OriginPro 8.5 software (OriginLab).

Immunohistochemistry—P10 pups were deeply anesthetized with isoflurane and then perfused transcardially, first with PBS (pH 7.4) and with 4% paraformaldehyde (PFA) dissolved in PBS. The brains were removed and postfixed in 4% PFA overnight at 4°C, and then were coronally sectioned (40 μm thick) using a vibratome (Leica Biosystems). Tyrosine hydroxylase (TH) staining was accomplished as follows: (1) rinse 40 μm-thick slices in PBS

(pH 7.4) three time; (2) block slices in 10% normal goat serum (Thermo Fisher, Cat. #: 50062Z) with 0.1% Triton X-100 (Sigma-Aldrich, Cat. #: T8787) in PBS for 1 h at room temperature; (3) incubate slices in rabbit polyclonal anti-TH primary antibody (1:700 in PBS; Sigma-Aldrich, Cat. #: T8700) for 24 h at 4°C (4) rinse slices in PBS three times; (5) incubate slices in Cy3-conjugated goat anti-rabbit IgG (1:100 in PBS, Jackson ImmunoResearch Laboratories, Cat. #: 111-165-003) and DAPI (1:1000) for 2 h at room temperature on a rotary shaker; (6) rinse slices in PBS three times and mount with an Aqua-Poly/Mount solution (Polysciences). TH-positive fibers in the cortex were imaged using a confocal microscope (Zeiss LSM800) and quantified by measuring the optical density of TH-immunofluorescence using MATLAB (Mathworks).

Behavioral Assays—Experiments were conducted during the light phase of the light/dark cycle between 10 AM and 4 PM using 4–9 weeks old mice except for a locomotor activity from P10 pups. Mouse activity was videotaped by an overhead camera (DMK22AUC03, Imaging Source), and behavior was automatically recorded by behavior tracking software (ANY-maze tracking software, Stoelting; EthoVision XT, Noldus). Both female and male mice were used.

Sociability text.: Sociability test was performed using a custom made rectangular, three-chamber box. Each chamber is 38 cm × 20 cm × 20 cm, with an open central compartment for free access to each chamber. A wire cup-like container (diameter: 8 cm) was place in each lateral compartment. During habituation, the experimental (subject) mouse was allowed to explore the three chambers for 5 minutes. After the habituation period, the lateral compartments were isolated using two plexiglass inserts, with the experimental mouse in the central compartment. The ‘stranger’ mouse was then gently placed inside the wire cup-like container located in one of the lateral compartments and the inserts between the compartments were removed to allow the subject mouse to explore each of the three compartments for 10 minutes. Time spent in each compartment was automatically recorded.

Open-field exploration.: Open field exploration was performed with ANY-box (Stoelting Co., IL, USA), a transparent multi-configuration behavior apparatus (40 cm × 40 cm × 40 cm). The open field arena was divided into a grid of equally sized areas (sides and center). To begin the experiment, a mouse was gently placed in the center of the arena and was allowed to explore the arena for 10 minutes. The location and activity of the mouse were recorded.

Light-dark exploration.: The mouse was placed centrally into the brightly illuminated compartment of a two-chamber box (40 cm × 40 cm × 40 cm) divided into two compartments by a dark partition with a small aperture at the bottom center (ANY-box, Stoelting Co., IL, USA). Mice were allowed to freely explore the chamber for 10 min while time spent in the each compartment were recorded.

Elevated plus maze.: Elevated plus maze was conducted in a custom-made apparatus that consists of a cross-shaped maze with a length of 50 cm and 7 cm width elevated 40 cm from the floor. Two arms were enclosed with 15-cm high walls, while the remaining two arms were unprotected. Each mouse was placed in the central area of the maze with open access

to any arm. The entire session was recorded and time spent in each arm was analyzed during the 10 min exploration time.

Locomotor activity.: Locomotor activity was measured for 10 min at P10 pups in an open field box (61 cm × 61 cm × 10 cm). Testing was conducted in the dark cycle with the absence of food and water. Mice were initially placed at the center of the box. Locomotor activity was recorded and analyzed by a behavior tracking software (EthoVision XT, Noldus).

Pharmacology—Stocks were prepared at 1,000 × (or greater) by dissolving Tetrodotoxin citrate, (R)-CPP, D-AP5, Eticlopride, and Bicuculline methochloride in water; NBQX and Haloperidol in DMSO; SCH23390 and Quinpirole in PBS; 6-OHDA in PBS containing ascorbic acid (0.25%). All drugs were from Tocris unless otherwise noted.

QUANTIFICATION AND STATISTICAL ANALYSIS

Quantification of spine density—All distinct protrusions emanating from the dendritic shaft, regardless of shape, were counted and measured in images from the red (tdTomato) or green (GFP) channel using ImageJ (NIH). For all cells included in our analysis, overall spine density did not significantly change over the 1 hour imaging session (data not shown). This ensured that the spine density being examined did not take place due to a general decrease in cell health, as widespread spine/filopodia-like structures can form when cell health is compromised. Filopodia (protrusions with length/neck width ratio, > 3; head width/neck width ratio, < 1.2) were excluded from the analysis. All images shown are maximum projections of 3D image stacks after applying a median filter (2 × 2) to the raw image data.

Statistical analysis—All statistics were calculated across cells. Error bars represent standard error of the mean and significance was set at $p = 0.05$ (Student's two-tailed t test). Single and double asterisks indicate $p < 0.05$ and $p < 0.01$, respectively. n.s., not significant.

Supplementary Material

Refer to Web version on PubMed Central for supplementary material.

ACKNOWLEDGMENTS

We thank members of the Kwon laboratory for helpful discussions and Long Yan for help with the two-photon microscope setup. This work was supported by the Max Planck Florida Institute for Neuroscience (to H.-B.K.), the National Institutes of Health (R01MH107460 and DP1MH119428 to H-B.K., R01MH124778 and R21MH126073 to W.C.O., and T32 NS 099042 to R.O.), a Brain and Behavior Research Foundation NARSAD Young Investigator Award (to W.C.O.), a Brain Research Foundation seed grant (to W.C.O.), and a CSU/CU-Pilot collaboration award (to W.C.O.).

REFERENCES

Arnsten AF (2009). Stress signalling pathways that impair prefrontal cortex structure and function. Nat. Rev. Neurosci 10, 410–422. [PubMed: 19455173]

Arnsten AF (2015). Stress weakens prefrontal networks: molecular insults to higher cognition. Nat. Neurosci 18, 1376–1385. [PubMed: 26404712]

Authement ME, Kodangattil JN, Gouty S, Rusnak M, Symes AJ, Cox BM, and Nugent FS (2015). Histone Deacetylase Inhibition Rescues Maternal Deprivation-Induced GABAergic Metaplasticity through Restoration of AKAP Signaling. Neuron 86, 1240–1252. [PubMed: 26050042]

Berger B, Gaspar P, and Verney C (1991). Dopaminergic innervation of the cerebral cortex: unexpected differences between rodents and primates. Trends Neurosci. 14, 21–27. [PubMed: 1709528]

Bick J, and Nelson CA (2016). Early Adverse Experiences and the Developing Brain. Neuropsychopharmacology 41, 177–196. [PubMed: 26334107]

Bosch M, and Hayashi Y (2012). Structural plasticity of dendritic spines. Curr. Opin. Neurobiol 22, 383–388. [PubMed: 21963169]

Brown SM, Henning S, and Wellman CL (2005). Mild, short-term stress alters dendritic morphology in rat medial prefrontal cortex. Cereb. Cortex 15, 1714–1722. [PubMed: 15703248]

Burke AR, and Miczek KA (2014). Stress in adolescence and drugs of abuse in rodent models: role of dopamine, CRF, and HPA axis. Psychopharmacology (Berl.) 231, 1557–1580. [PubMed: 24370534]

Chen SX, Kim AN, Peters AJ, and Komiyama T (2015). Subtype-specific plasticity of inhibitory circuits in motor cortex during motor learning. Nat. Neurosci 18, 1109–1115. [PubMed: 26098758]

Chen CC, Lu J, Yang R, Ding JB, and Zuo Y (2018). Selective activation of parvalbumin interneurons prevents stress-induced synapse loss and perceptual defects. Mol. Psychiatry 23, 1614–1625. [PubMed: 28761082]

Clarkson RL, Liptak AT, Gee SM, Sohal VS, and Bender KJ (2017). D3 Receptors Regulate Excitability in a Unique Class of Prefrontal Pyramidal Cells. J. Neurosci 37, 5846–5860. [PubMed: 28522735]

Cook SC, and Wellman CL (2004). Chronic stress alters dendritic morphology in rat medial prefrontal cortex. J. Neurobiol 60, 236–248. [PubMed: 15266654]

Deutch AY, and Roth RH (1990). The determinants of stress-induced activation of the prefrontal cortical dopamine system. Prog. Brain Res 85, 367–402, discussion 402–403. [PubMed: 2094906]

Friedman AK, Walsh JJ, Juarez B, Ku SM, Chaudhury D, Wang J, Li X, Dietz DM, Pan N, Vialou VF, et al. (2014). Enhancing depression mechanisms in midbrain dopamine neurons achieves homeostatic resilience. Science 344, 313–319. [PubMed: 24744379]

Hamilton AM, Oh WC, Vega-Ramirez H, Stein IS, Hell JW, Patrick GN, and Zito K (2012). Activity-dependent growth of new dendritic spines is regulated by the proteasome. Neuron 74, 1023–1030. [PubMed: 22726833]

Holly EN, and Miczek KA (2016). Ventral tegmental area dopamine revisited: effects of acute and repeated stress. Psychopharmacology (Berl.) 233, 163–186. [PubMed: 26676983]

Holtmaat A, and Svoboda K (2009). Experience-dependent structural synaptic plasticity in the mammalian brain. Nat. Rev. Neurosci 10, 647–658. [PubMed: 19693029]

Holtmaat A, Wilbrecht L, Knott GW, Welker E, and Svoboda K (2006). Experience-dependent and cell-type-specific spine growth in the neocortex. Nature 441, 979–983. [PubMed: 16791195]

Izquierdo A, Wellman CL, and Holmes A (2006). Brief uncontrollable stress causes dendritic retraction in infralimbic cortex and resistance to fear extinction in mice. J. Neurosci 26, 5733–5738. [PubMed: 16723530]

Jacob SN, and Nienborg H (2018). Monoaminergic Neuromodulation of Sensory Processing. Front. Neural Circuits 12, 51. [PubMed: 30042662]

Katz LC, and Shatz CJ (1996). Synaptic activity and the construction of cortical circuits. Science 274, 1133–1138. [PubMed: 8895456]

Kessler RC, Davis CG, and Kendler KS (1997). Childhood adversity and adult psychiatric disorder in the US National Comorbidity Survey. Psychol. Med 27, 1101–1119. [PubMed: 9300515]

Kim JJ, and Diamond DM (2002). The stressed hippocampus, synaptic plasticity and lost memories. Nat. Rev. Neurosci 3, 453–462. [PubMed: 12042880]

Kolb B, Mychasiuk R, Muhammad A, Li Y, Frost DO, and Gibb R (2012). Experience and the developing prefrontal cortex. Proc. Natl. Acad. Sci. USA 109 (Suppl 2), 17186–17193. [PubMed: 23045653]

Kwon HB, and Sabatini BL (2011). Glutamate induces de novo growth of functional spines in developing cortex. Nature 474, 100–104. [PubMed: 21552280]

Lammel S, Ion DI, Roeper J, and Malenka RC (2011). Projection-specific modulation of dopamine neuron synapses by aversive and rewarding stimuli. Neuron 70, 855–862. [PubMed: 21658580]

Lammel S, Lim BK, and Malenka RC (2014). Reward and aversion in a heterogeneous midbrain dopamine system. Neuropharmacology 76 Pt B, 351–359. [PubMed: 23578393]

Lupien SJ, McEwen BS, Gunnar MR, and Heim C (2009). Effects of stress throughout the lifespan on the brain, behaviour and cognition. Nat. Rev. Neurosci 10, 434–445. [PubMed: 19401723]

Money KM, and Stanwood GD (2013). Developmental origins of brain disorders: roles for dopamine. Front. Cell. Neurosci 7, 260. [PubMed: 24391541]

Oh WC, Hill TC, and Zito K (2013). Synapse-specific and size-dependent mechanisms of spine structural plasticity accompanying synaptic weakening. Proc. Natl. Acad. Sci. USA 110, E305–E312. [PubMed: 23269840]

Oh WC, Lutzu S, Castillo PE, and Kwon HB (2016). De novo synaptogenesis induced by GABA in the developing mouse cortex. Science 353, 1037–1040. [PubMed: 27516412]

Peters AJ, Chen SX, and Komiyama T (2014). Emergence of reproducible spatiotemporal activity during motor learning. Nature 510, 263–267. [PubMed: 24805237]

Polter AM, and Kauer JA (2014). Stress and VTA synapses: implications for addiction and depression. Eur. J. Neurosci 39, 1179–1188. [PubMed: 24712997]

Radley JJ, Sisti HM, Hao J, Rocher AB, McCall T, Hof PR, McEwen BS, and Morrison JH (2004). Chronic behavioral stress induces apical dendritic reorganization in pyramidal neurons of the medial prefrontal cortex. Neuroscience 125, 1–6. [PubMed: 15051139]

Radley JJ, Rocher AB, Rodriguez A, Ehlenberger DB, Dammann M, McEwen BS, Morrison JH, Wearne SL, and Hof PR (2008). Repeated stress alters dendritic spine morphology in the rat medial prefrontal cortex. J. Comp. Neurol 507, 1141–1150. [PubMed: 18157834]

Rentesi G, Antoniou K, Marselos M, Syrrou M, Papadopoulou-Daifoti Z, and Konstandi M (2013). Early maternal deprivation-induced modifications in the neurobiological, neurochemical and behavioral profile of adult rats. Behav. Brain Res 244, 29–37. [PubMed: 23395600]

Robinson SE, and Sohal VS (2017). Dopamine D2 Receptors Modulate Pyramidal Neurons in Mouse Medial Prefrontal Cortex through a Stimulatory G-Protein Pathway. J. Neurosci 37, 10063–10073. [PubMed: 28912160]

Shin S, Pribiag H, Lilascharoen V, Knowland D, Wang XY, and Lim BK (2018). Drd3 Signaling in the Lateral Septum Mediates Early Life Stress-Induced Social Dysfunction. Neuron 97, 195–208.e6. [PubMed: 29276054]

Shioda N, Yabuki Y, Wang Y, Uchigashima M, Hikida T, Sasaoka T, Mori H, Watanabe M, Sasahara M, and Fukunaga K (2017). Endocytosis following dopamine D_2 receptor activation is critical for neuronal activity and dendritic spine formation via Rabex-5/PDGFRβ signaling in striatopallidal medium spiny neurons. Mol. Psychiatry 22, 1205–1222. [PubMed: 27922607]

Shu Y, and Xu T (2017). Chronic Social Defeat Stress Modulates Dendritic Spines Structural Plasticity in Adult Mouse Frontal Association Cortex. Neural Plast. 2017, 6207873. [PubMed: 28197343]

Silverman JL, Yang M, Lord C, and Crawley JN (2010). Behavioural phenotyping assays for mouse models of autism. Nat. Rev. Neurosci 11, 490–502. [PubMed: 20559336]

Spruston N (2008). Pyramidal neurons: dendritic structure and synaptic integration. Nat. Rev. Neurosci 9, 206–221. [PubMed: 18270515]

Tost H, Champagne FA, and Meyer-Lindenberg A (2015). Environmental influence in the brain, human welfare and mental health. Nat. Neurosci 18, 1421–1431. [PubMed: 26404717]

Tritsch NX, and Sabatini BL (2012). Dopaminergic modulation of synaptic transmission in cortex and striatum. Neuron 76, 33–50. [PubMed: 23040805]

Tschida KA, and Mooney R (2012). Deafening drives cell-type-specific changes to dendritic spines in a sensorimotor nucleus important to learned vocalizations. Neuron 73, 1028–1039. [PubMed: 22405211]

Wanat MJ, Hopf FW, Stuber GD, Phillips PE, and Bonci A (2008). Corticotropin-releasing factor increases mouse ventral tegmental area dopamine neuron firing through a protein kinase C-dependent enhancement of Ih. J. Physiol 586, 2157–2170. [PubMed: 18308824]

Wang SS, Kloth AD, and Badura A (2014). The cerebellum, sensitive periods, and autism. Neuron 83, 518–532. [PubMed: 25102558]

Weber MA, Graack ET, Scholl JL, Renner KJ, Forster GL, and Watt MJ (2018). Enhanced dopamine D2 autoreceptor function in the adult prefrontal cortex contributes to dopamine hypoactivity following adolescent social stress. Eur. J. Neurosci 48, 1833–1850. [PubMed: 29904960]

Xu T, Yu X, Perlik AJ, Tobin WF, Zweig JA, Tennant K, Jones T, and Zuo Y (2009). Rapid formation and selective stabilization of synapses for enduring motor memories. Nature 462, 915–919. [PubMed: 19946267]

Yizhar O, Fenno LE, Prigge M, Schneider F, Davidson TJ, O'Shea DJ, Sohal VS, Goshen I, Finkelstein J, Paz JT, et al. (2011). Neocortical excitation/inhibition balance in information processing and social dysfunction. Nature 477, 171–178. [PubMed: 21796121]

Highlights

- Early-life stress (ELS) enhances excitation-inhibition ratio in prefrontal cortex (PFC)
- ELS increases intrinsic excitability of PFC-projecting VTA dopaminergic neurons
- ELS-induced alterations in the developing PFC and VTA are long lasting
- Dopamine D2 receptor signaling mediates ELS-induced synaptic change in the PFC

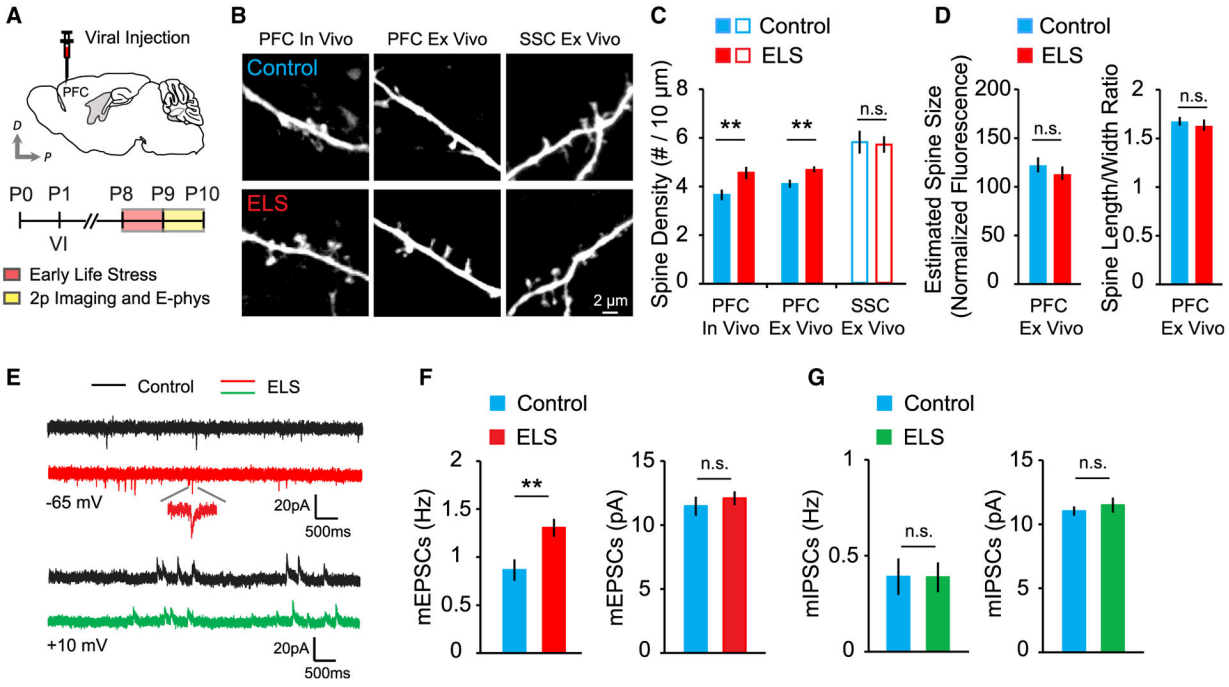

Figure 1. A single episode of ELS increases the synaptic excitation-to-inhibition ratio

(A) Schematic of adeno-associated virus (AAV) injection and experimental timeline.

(B) Images of dendrites from layer 2/3 pyramidal neurons from the PFC and SSC of control and ELS mice.

(C) Summary graph of spine density *in vivo* (control, 27 cells, 6 mice; ELS, 25 cells, 5 mice) and *in vitro* (control, 18 cells, 4 mice; ELS, 18 cells, 4 mice) in the PFC and SSC (control, 10 cells, 3 mice; ELS, 11 cells, 3 mice).

(D) Quantitative analysis of the estimated spine size and spine length-to-width ratio (control, 18 cells, 4 mice; ELS, 18 cells, 4 mice).

(E) Representative traces of mEPSCs and mIPSCs.

(F) Quantification of the frequency (left) and amplitude (right) of mEPSCs in control (14 cells, 3 mice) and ELS (15 cells, 3 mice) mice.

(G) Summary graph of mIPSC frequency (left) and amplitude (right) in control (14 cells, 4 mice) and ELS (15 cells, 4 mice) mice.

**p < 0.01. Error bars represent SEM. n.s., not significant.

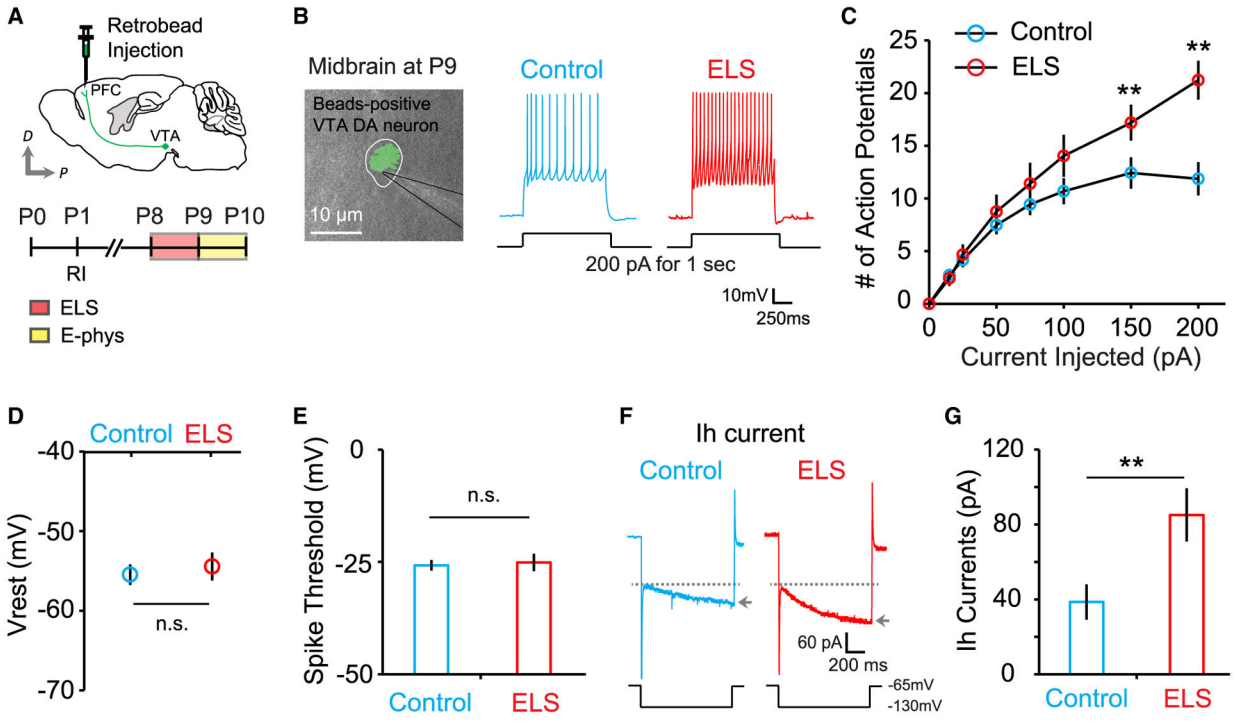

Figure 2. Mesoprefrontal VTA DA neurons of ELS mice exhibit increased intrinsic excitability

(A) Schematic of RetroBead injection and experimental timeline.

(B) An overlay of fluorescent and differential interference contrast (DIC) images shows a retrogradely labeled (green beads), mesoprefrontal, putative VTA DA neuron. Example traces show a stimulus train of action potentials evoked by current injection of 200 pA for 1 s.

(C) Summary data plotting the number of action potentials in control (23 cells, 6 mice) and ELS (15 cells, 3 mice) mice.

(D and E) Average resting membrane potential (D; control, 23 cells, 6 mice; ELS, 15 cells, 3 mice) and spike threshold (E; control, 23 cells, 6 mice; ELS, 14 cells, 3 mice) in control and ELS mice.

(F) Representative traces of I_h currents measured by hyperpolarizing voltage pulse (1 s duration) to −130 mV (arrows) from a holding potential of −65 mV (dotted lines).

(G) Quantification of I_h measured from control (25 cells, 6 mice) and ELS (12 cells, 3 mice) mice.

**p < 0.01. Error bars represent SEM.

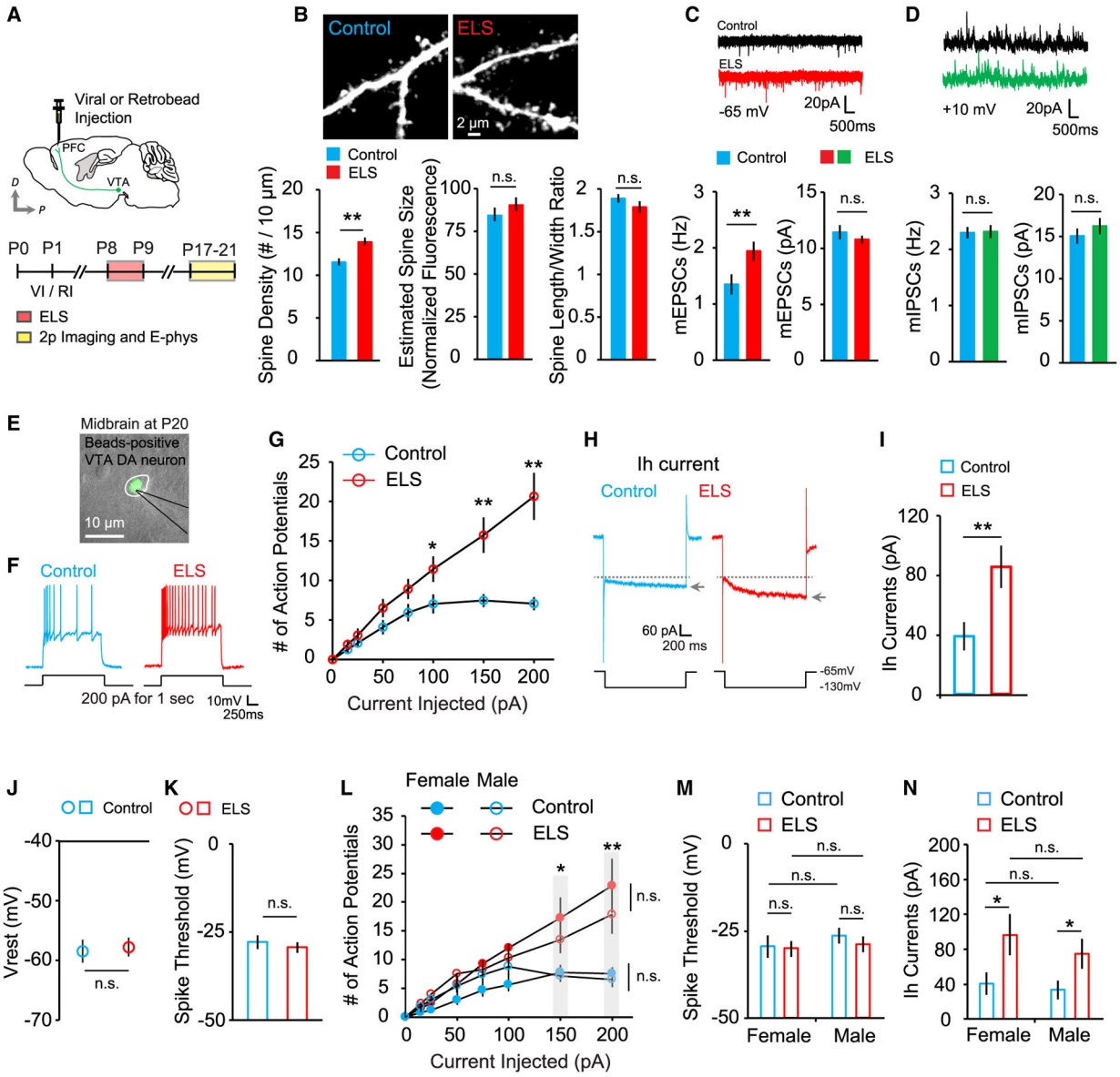

Figure 3. ELS-induced enhanced excitatory synapse density in the PFC and increased activity of PFC-projecting VTA DA neurons are long lasting

(A) Schematic of the experimental timeline.

(B) Images of dendrites from layer 2/3 pyramidal neurons of control and ELS mice and quantification of spine density (left), estimated spine size (center), and spine length-to-width ratio (right) in control (13 cells, 3 mice) and ELS (13 cells, 3 mice) mice.

(C) Representative mEPSC traces and average mEPSC frequency (left) and amplitude (right) in control (13 cells, 3 mice) and ELS (14 cells, 3 mice) mice.

(D) Example mIPSC traces and average mIPSC frequency (left) and amplitude (right) in control (13 cells, 3 mice) and ELS (14 cells, 3 mice) mice.

(E) An overlay of fluorescence and DIC images.

(F) Representative voltage responses to step current injection of 200 pA for 1 s.

(G) Summary graph plotting the number of action potentials against current injection in control (21 cells, 5 mice) and ELS (25 cells, 5 mice) mice.
(H) Example traces of I_h currents.
(I–K) Summary graphs of (I) I_h current, (J) resting membrane potential, and (K) spike threshold in control (24 cells, 5 mice) and ELS (23 cells, 5 mice) mice.
(L–N) Quantification of (L) action potential spikes, (M) average spike threshold, and (N) I_h currents measured in female and male control (3 mice each) and ELS (4 mice each) mice.
**$p < 0.01$, *$p < 0.05$. Error bars represent SEM.

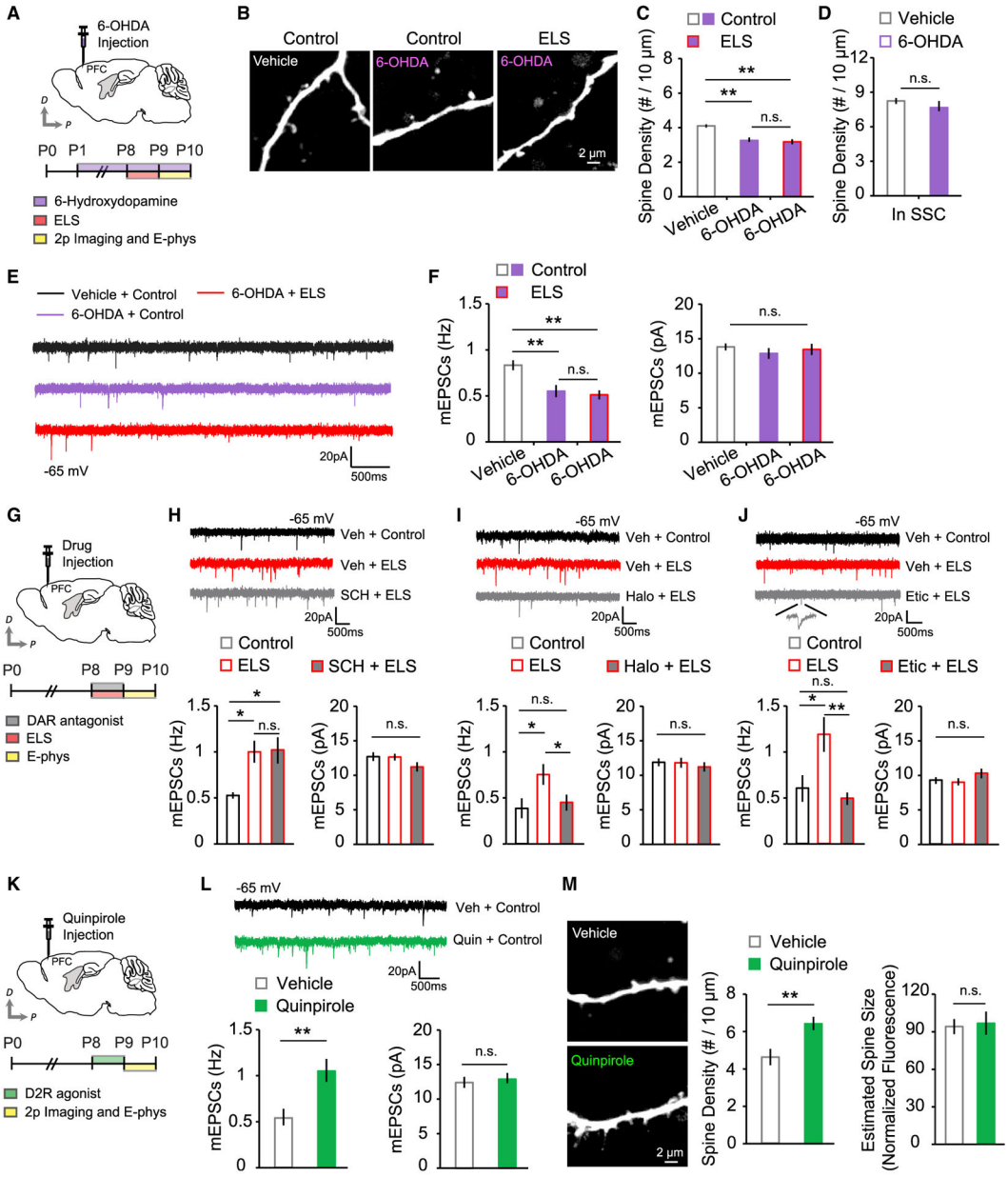

Figure 4. DA D2 receptor signaling in the PFC mediates ELS-induced structural and functional alterations of excitatory synapses

(A) Schematic of 6-OHDA injection and experimental timeline.

(B) Images of dendrites under each condition.

(C) Quantification of PFC spine density in vehicle-treated control (12 cells, 3 mice), 6-OHDA-treated control (18 cells, 3 mice), and 6-OHDA-treated ELS (15 cells, 3 mice) mice.

(D) Average SSC spine density in vehicle-treated (10 cells, 3 mice) and 6-OHDA-treated control (10 cells, 3 mice) mice.

(E) Example mEPSC traces.

(F) Quantitative analysis of mEPSC frequency (left) and amplitude (right) in vehicle-treated control (19 cells, 3 mice), 6-OHDA-treated control (22 cells, 3 mice), and 6-OHDA-treated ELS (21 cells, 3 mice) mice.

(G) Schematic of drug injection and experimental timeline.
(H) Example mEPSC traces for the SCH23390 test and average mEPSC frequency (left) and amplitude (right) in vehicle-treated control (9 cells, 3 mice), vehicle-treated ELS (12 cells, 5 mice), and SCH23390-treated ELS (14 cells, 5 mice) mice.
(I) Example mEPSC traces in the haloperidol test and average mEPSC frequency (left) and amplitude (right) in vehicle-treated control (9 cells, 3 mice), vehicle-treated ELS (14 cells, 6 mice), and haloperidol-treated ELS (14 cells, 6 mice) mice.
(J) Example mEPSC traces in the eticlopride test and average mEPSC frequency (left) and amplitude (right) in vehicle-treated control (16 cells, 3 mice), vehicle-treated ELS (10 cells, 3 mice), and eticlopride-treated ELS (17 cells, 3 mice) mice.
(K) Schematic of D2 receptor agonist injection and experimental timeline.
(L) Representative mEPSC traces and quantification of mEPSC frequency (left) and amplitude (right) in vehicle-treated (19 cells, 7 mice) and quinpirole-treated (22 cells, 7 mice) mice.
(M) Images of PFC dendrites from vehicle- or quinpirole-treated mice and quantification of PFC spine density and estimated spine size in the vehicle (12 cells, 3 mice) and quinpirole (13 cells, 3 mice) groups.
**$p < 0.01$, *$p < 0.05$. Error bars represent SEM.

KEY RESOURCES TABLE

REAGENT or RESOURCE	SOURCE	IDENTIFIER
Antibodies		
Rabbit polyclonal anti-TH primary antibody	Sigma-Aldrich	Cat# T8700; RRID: AB_1080430
Cy3-conjugated goat anti-rabbit IgG	Jackson ImmunoResearch Laboratories	Cat# 111-165-003; RRID: AB_2338000
Bacterial and virus strains		
pAAV-CAG-tdTomato	Gift from Edward Boyden	Addgene# 59462
AAV1-CAG-Flex-tdTomato-WPRE-bGH	Gift from Hongkui Zeng	Addgene# 51503
Chemicals, peptides, and recombinant proteins		
Green Retrobeads	Lumafluor	Green Retrobeads IX
Tetrodotoxin citrate	Tocris	Cat# 1069
(R)-CPP	Tocris	Cat# 0247
D-APV	Tocris	Cat# 0106
Bicuculline methochloride	Tocris	Cat# 0131
NBQX	Tocris	Cat# 0373
Haloperidol hydrochloride	Tocris	Cat# 0931
SCH23390 hydrochloride	Tocris	Cat# 0925
Eticlopride hydrochloride	Tocris	Cat# 1847
(-)-Quinpirole hydrochloride	Tocris	Cat# 1061
6-OHDA	Tocris	Cat# 2547
Experimental models: Organisms/strains		
Mouse: C57BL/6NJ	Jackson Laboratories	005304
Mouse: DAT-IRES-Cre	Jackson Laboratories	006660
Software and algorithms		
ImageJ	NIH	https://imagej.nih.gov/ij/
pClamp	Molecular Devices	N/A
Prairie View	Bruker	N/A
MATLAB	MathWorks	N/A
EthoVision XT	Noldus	N/A
Any-maze video tracking software	Stoelting Co	N/A
Other		
Multiphoton microscope	Bruker	https://www.bruker.com/en.html
Ti::sapphire laser	Spectra Physics	MaiTai HP
10% normal goat serum	Thermo Fisher	Cat# 50062Z
Triton X-100	Sigma-Aldrich	Cat# T8787